JACS
JOURNAL OF THE AMERICAN CHEMICAL SOCIETY
pubs.acs.org/JACS
Article

Molecular Conformation in Charge Tunneling across Large-Area Junctions

Chuanshen Du, Sean R. Norris, Abhishek Thakur, Jiahao Chen, Brett VanVeller, and Martin Thuo*

Cite This: J. Am. Chem. Soc. 2021, 143, 13878−13886
Read Online
ACCESS | Metrics & More | Article Recommendations | Supporting Information

ABSTRACT: Self-assembled monolayers are predicated on thermodynamic equilibrium; hence, their properties project accessible relaxation pathways. Herein, we demonstrate that charge tunneling correlates with conformational degrees of freedom(s). Results from open chain and cyclic head groups show that, as expected, distribution in tunneling data correlates with the orientation of the head group, akin to the odd−even effect and more importantly the degree of conformational freedom, but fluctuates with applied bias. Trends in nature of distributions in current density illuminate the need for higher statistical moments in understanding these rather dynamic systems. We employ skewness, kurtosis, and estimation plots to show that the conformational degree of freedom in the head group significantly amplifies the odd−even effect and may lead to enhanced or perturbed tunneling based on whether the head group is on an odd- or even-parity spacer.

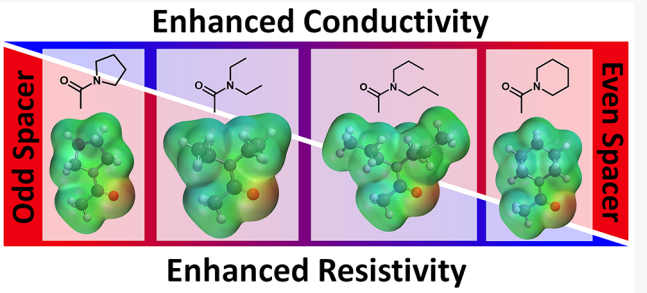

INTRODUCTION

The unimolecular nature of self-assembled monolayers (SAMs) provides an excellent opportunity to study structure−property relationships of charge tunneling across molecular systems.[2−11] Apart from the effects of surface roughness and identity of the substrate,[4,12] properties of the molecule making up the monolayer define barrier characteristics and supramolecular structure. Studies on structure-dependent charge transport across monolayers show that features such as chain length,[7,9,13−15] dipole moments,[16,17] SAM isomorphism,[18] SAM supramolecular structure,[14,19,20] contact geometry,[21] as well as conformational order[1,20] can affect charge transport across SAMs. Among all these properties, molecular conformation is one of the least explored because it is difficult to isolate since conformational changes can be associated with other major structural changes like gauche defects. Charge transport across SAM junctions is commonly modeled using Simmons' equation,[22,23] which in its simplest form is described as

$$J = J_0 e^{-\beta d} \tag{1}$$

where d is the thickness of the barrier; β is the length-dependent decay constant; J is current density; and J_0 is current density when $d = 0$. Simmons' model is focused on the electronic properties (β and J_0) and physical length (d) of the barrier[24−26] and hence fails to capture stereoelectronic properties of the molecule(s) constituting the barrier. Stereoelectronic considerations (spatial relations in interaction between molecular orbitals or electronic components) are important since tunneling in SAMs is a through-bond process. The through-bond process, therefore, imposes cases where geometric constraints on charge transport occur[20] and needs to be identified and considered for a complete understanding of molecular electronics. Given the stochastic nature of the possible molecular conformation, especially with high degrees of rotational freedom (e.g., in linear hydrocarbons), barrier(s) to charge injection and characteristics of the tunnel path can lead to differences in tunneling probability. Given this stochasticity, Simmons' model should be described as a summation of the disparate geometric molecular states as

$$J = \sum_{i=1}^{n} N_i J_{0-i} e^{-\beta_i d_i} \tag{2}$$

where J_{0-i}, β_i, and d_i are parameters describing the i^{th} possible state for the molecule, and N_i are the number of molecules in each state during measurement. Given the complexity in obtaining N_i, the probabilistic Landauer formula (eq 3) has been adopted as an alternative to the Simmons' equation.

$$G = \frac{e^2}{\pi h} T(E) \tag{3}$$

Received: June 25, 2021
Published: August 20, 2021

https://doi.org/10.1021/jacs.1c06622
J. Am. Chem. Soc. 2021, 143, 13878−13886

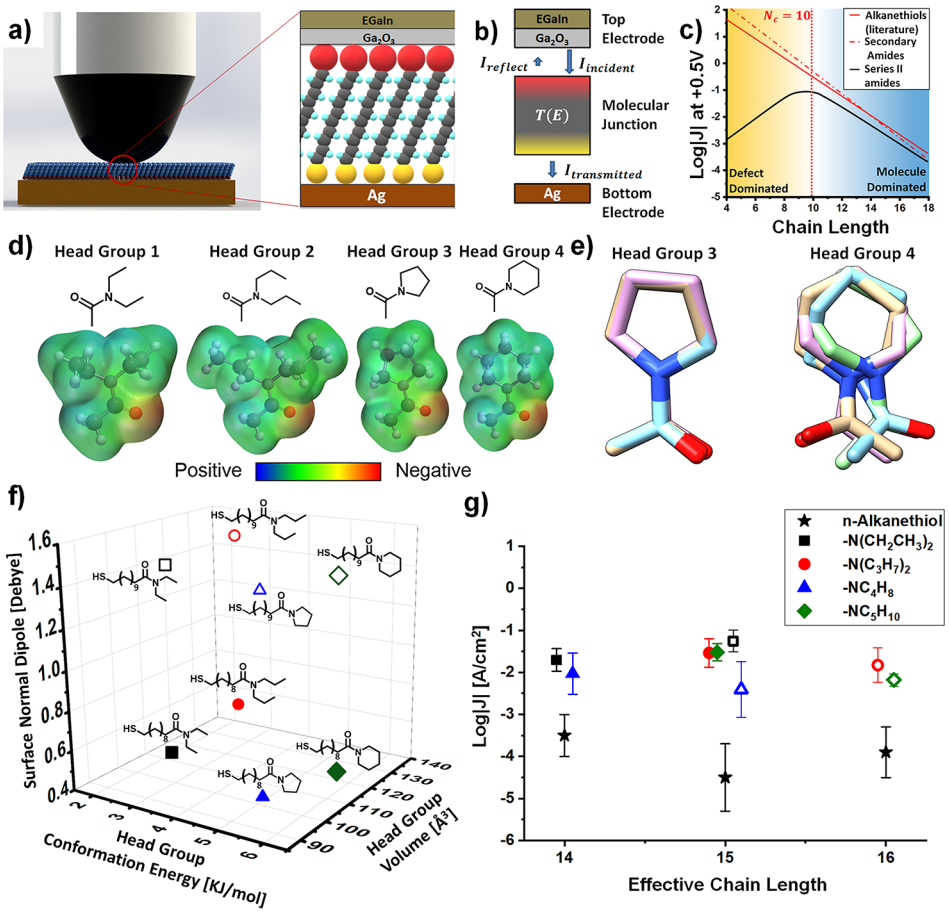

Figure 1. (a) Schematic of the charge-tunneling system used to characterize SAMs. (b) Proposed theoretical schematic of charge transport across SAMs. (c) Evolution of current density at 0.5 V for *n*-alkanethiolate and amide SAMs.[1] (d) Functional groups, and their electrostatic potential maps, used to in this study. (e) Computer simulation revealing the conformation degrees of freedom for two of the head groups. (f) Classification of molecules based on conformation energy, volume, and dipole moment of the head group. (g) Current density at 0.5 V for SAMs in this work compared to analogous n-alkanethiols.

$$T(E) = \frac{\Gamma_1\Gamma_2}{\left(\frac{\Gamma_1+\Gamma_2}{2}\right)^2 + (E - E_{\mathrm{HOMO}})^2} \tag{4}$$

where $T(E)$ is transmission probability, and Γ is the coupling strength between the molecule and the electrode. Figure 1a schematically illustrates an ideal EGaIn-based tunnel junction, while Figure 1b illustrates the $T(E)$-dominated transmission and back scattering of applied charge. Given that $\Gamma_1 \gg \Gamma_2$ (with electrode 1 being from the chemisorbed Ag and 2 the physisorbed EGaIn interfaces) and that the energy offset ($\varepsilon = E_F - E_{HOMO}$) is much larger than Γ_1, $T(E) \approx \Gamma_1\Gamma_2/\varepsilon$.[27−29] This simplification implies that charge transport is highly dependent on the weakly coupling electrode, highlighting the importance of the nature of the physisorbed SAM interface.

Reliance on the transmission probability (eq 4) emphasizes the role of molecule−electrode coupling (Γ) and the underlying stochasticity but fails to capture dynamic geometric perturbations due to applied bias (e.g., from joule heating).[30] The geometric perturbations we highlight here are rooted in limitations due to fixed bond angles and bond lengths (molecular conformations) that we believe are essential in understanding charge injection from an electrode to the molecule—especially where a Van der Waals interface exists. This type of interface is present at the physisorbed contact of EGaIn-based large-area tunneling junctions (Figure 1a).

Appreciating the complexity in SAMs and associated molecule−electrode interfaces has inspired advances in data characterization and interpretation. Earlier studies on tunneling across SAMs, for example, relied on lower statistical moments at a single bias,[9,13,16,23] which has been shown to be insufficient in capturing the dynamic complex nature of these junctions.[17,18,31] By simply deploying higher (third and fourth) statistical moments, we illustrated dynamic structural- and bias-dependent intramolecular Keesom (dipole) interactions. We have previously shown that bias-dependent trends of skewness/kurtosis can reveal stereoelectronic changes (dipole reorientation) in SAMs during charge tunneling.[17,18,31] It is therefore apparent that the role of structural changes that can result from the applied field should be investigated, and their role in tunneling should be describe if large-area tunneling junctions are to become widely useful.

EXPERIMENTAL SECTION

All chemicals and reagents were purchased from Sigma-Aldrich; 200-proof ethanol was purchased from Decon Laboratories, while gases were purchased from Airgas.

Computational Method. In the current work, simulations were performed using the following multistep strategy. Initially, MD simulations on each head group were performed in vacuum to analyze the physical movements of atoms and molecules. In the next step cluster analysis was performed to obtain the most dominant

https://doi.org/10.1021/jacs.1c06622
J. Am. Chem. Soc. 2021, 143, 13878−13886

conformations of each head. In the final step, QM analysis was used to compare the energy and stability of each conformer. The 100 ns molecular dynamics simulations were done to generate different conformations of the heads and estimate the energy barrier for each head. The three-dimensional structure of heads was optimized without any geometrical constraints at the B3LYP-D3/6-31G** level. Antechamber, an inbuilt tool in Amber, was used to calculate RESP charges and to make topology files of all molecules.[32] The all-atom MD simulations of each head were performed using the AMBER program utilizing the GAFF2 force field.[33] The CPU version of the sander engine which comes integrated with Amber16 tools was adopted in this study.[3] Each system was minimized over 10 000 steps using the conjugate gradient (CG) method with a constant dielectric medium instead of implicit or explicit solvents. The minimized structures were gradually heated from 0 to 300 K using a constant NVT ensemble over 500 ps with a Berendsen temperature coupling and a nonbonded "cutoff" of 999 Å. Under the same NVT ensemble setup at 300 K with no periodic boundary conditions and 1 fs of time step, 100 ns of the production run was carried out. After the MD simulations were performed, the 100 ns of trajectory for each system was clustered using the "average-linkage" algorithm, generating the top 10 most dominating clustered structures for each system.[34,35] In the final step, the most dominating structures were further subjected to DFT single-point energy calculations to estimate the gas-phase energy for all possible conformers.

ESP and group volumes were calculated using Spartan Student v7.27. All head group structures were calculated as the equilibrium geometry in gas with density functional EDF2 using a polarization basis setting of 6-31G*. Calculated orbitals and energies were printed generating both ESP map and volume.

Chemical Synthesis. All molecules were synthesized from the corresponding brominated carboxylic acids, based on the carbon chain length (Scheme 1). Conversion of the carboxylic acid was

Scheme 1. Schematic Illustration of the Synthesis of Dialkyl Amides Used in This Study[a]

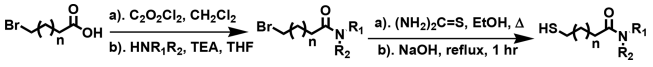

[a]A carboxylic acid is converted to an acyl chloride followed by amidation and installation of the thiol.

achieved by reaction with oxalyl chloride with catalytic *N*,*N*-dimethylformamide. Crude product was able to be used to react with the correct amines to form the bromo amide product. Following purification, thiourea allows substitution of the bromine to the thiol. Dithiothreitol with triethylamine allowed reduction of disulfides that can form, ensuring free thiol products. ^{1}H and ^{13}C NMR data are available in the Supporting Information.

Substrate Preparation and SAM Fabrication. The substrates used were prepared in house as previously reported.[13] In brief, a 200 nm Ag thin film was deposited on a fresh Si wafer (111) using e-beam evaporation. Template stripping was then performed to reveal the Ag−Si interface.

To fabricate SAMs on Ag surfaces, we follow the same procedure as previously reported.[13] In brief, the template-stripped substrates were precleaned with ethanol and then placed in a vial containing 3 mmol of alkanethiol in 5 mL of ethanol. The substrate and solution were incubated, under Argon gas, for 3 h. The substrates with SAMs were then rinsed with ethanol and dried with nitrogen gas.

Preparation of a Smoothened EGaIn Top Electrode. A polished EGaIn (99.99%, Sigma-Aldrich) conical tip was formed as previously reported.[2,17] In brief, a droplet of EGaIn pushed from a syringe onto a surface on which EGaIn would stick. The syringe was slowly pulled away using a micromanipulator (Narishige You-1) from the surface to form a conical-shaped tip after breaking the droplet. The conical tip was smoothened by dipping into 5% acetic acid (glacier, 99.7%) solution in ethanol for 2 min.

Electrical Measurement. Electrical measurements were conducted as previously reported.[2,17] A gold-coated tip was used to form a contact with the bottom electrode (Ag substrate) with a micropositioner (Signatone). A smoothened EGaIn electrode was brought in contact with the SAM with a micromanipulator to form a junction (physical contact). The measured diameter of the junction was used to estimate the area of the junction, assuming a full circular contact. Current density vs voltage data were collected in a sweeping bias from −0.5 V to 0.5 V, with a step size of 0.05 V. At least 20 scans were performed on each junction, and at least 20 junctions were studied per molecule.

RESULTS AND DISCUSSION

To delineate the effect of conformation dynamics at the electrode−SAM interface, we herein compare the effect of having open or closed (cyclic) amide head groups paying special attention to parity (odd−even) effect(s). To mitigate the effect of gauche defects, we anchor these amides with either a C_{10} or C_{11} alkyl thiol such that the overall SAMs are $\geq$ C_{14} *n*-alkylthiol analogue in length (Figure 1d).[10,30,36−39] Besides mitigating gauche defects, the length ensures solid-like (crystalline) ordering (Figure 1c).[10,30,36−39] We infer that this crystalline all-trans extended structure will allow for delineation of the effect of conformational order and its perturbation to tunneling of these homologous modifiers (Figure 1d). Considering the geometric consequences of introducing open and cyclic dialkyl amide head groups, we observe that though the amide dipole remains relatively unperturbed these analogues have significant differences in volume (Figure 1d). From the electrostatic potential maps, we observe that $V_{pyrrolidine} < V_{diethyl} < V_{piperidine} < V_{dipropyl}$. These moieties, however, have different degrees of conformation freedom that do not directly relate to the progression in volumetric change, suggesting that conformational degree of freedom is more aligned with structures (open vs cyclic) than volume—the latter being essential in SAM packing.[1] To confirm this inference, we applied molecular dynamics (MD) simulations and quantum mechanics (QM) analysis to generate different head group conformations and compute their energies, respectively. From simulation results, we confirmed the existence of a set of cluster structures with similar energies associated with each of the head groups (Figure S3 and Supporting Information Videos 1−4). The low-energy difference between different conformers (Supporting Information, Table S1), especially in head groups 1, 2, and 4, suggests that it can easily adopt other conformers, whereas, as expected for cyclic 5-membered rings, head group 3 has limited conformational changes (Supporting Information Table S1 and Figure S4). Based on the simulation results, and as expected, we confirm that the conformational degree of freedom for these head groups follows the order: $DOF_{pyrrolidine} < DOF_{piperidine} < DOF_{diethyl} < DOF_{dipropyl}$. For brevity, we schematically illustrate the differences in conformation cluster using pyrrolidine (3) and piperidine (4) (Figure 1e). For clarity, we summarize differences in the molecules based on head group volume, head group conformation degree of freedom, and surface normal dipole (Figure 1f). Besides the head groups, due to the well-known odd−even effect, the alkyl space must also be considered. The C_{10} alkanethiol backbone, for example, orients the amide dipole moment at 79.7° relative to the surface normal, while the C_{11} alkanethiol backbone orients an analogous dipole moment 120.3° relative to the surface normal. This study is, therefore, organized in two sets based on the underlying spacer alkyl thiol.

https://doi.org/10.1021/jacs.1c06622
J. Am. Chem. Soc. 2021, 143, 13878−13886

Charge tunneling across these homologues gives higher current than *n*-alkanethiols of equivalent length (Figure 1g). As expected, an increase in length leads to a decrease in current density except for the diethyl amides (Figure 1g). Surprisingly, pyrrolidine on a C_{11} chain showed the highest variance in average current density measured at 0.5 V, albeit lower than the equivalent *n*-alkanethiolate SAM (Figure 1g). We, therefore, infer that although there are significant differences in observed current densities at a single voltage a detailed analysis of these data, across all biases, is warranted if wholesome tunneling characteristics of these homologues, and related conformationally diverse analogues, are to be well understood.

General Trends. As previously reported, amides have a minimal effect on current density at a single voltage.[16] As shown in Figure 2, all C_{10}-based molecules had a current density around $10^{-1.7}$ A·cm^{-1} (left column, abbreviated 1^{E}–4^{E} with reference to the even spacer), while all C_{11}-based molecules yielded a current density around 10^{-2} A·cm^{-1} (right column, 1°–4° with reference to the even spacer). Although the heatmaps present the overall trends in the data, bias-to-bias fluctuations cannot be readily deduced. To capture the entire bias-dependent charge-tunneling behavior, we fitted a Gaussian curve to each applied bias. Figure 2b gives examples of such fits, and the remaining analogous fits are given in the Supporting Information (Figures S1 and S2). As shown in this representative sample, these Gaussian fits revealed that as the applied voltage changes the distribution of the current density uniquely shifts for each molecule. We can therefore infer that the head group's response to the applied bias varies and is unique to each one of them. The shape of the distributions (tails and peakedness) also changes with applied bias, further suggesting that the SAM is dynamic and hence nonlinearly responds to the applied field. Below, we systematically decouple the complexity revealed in these fits.

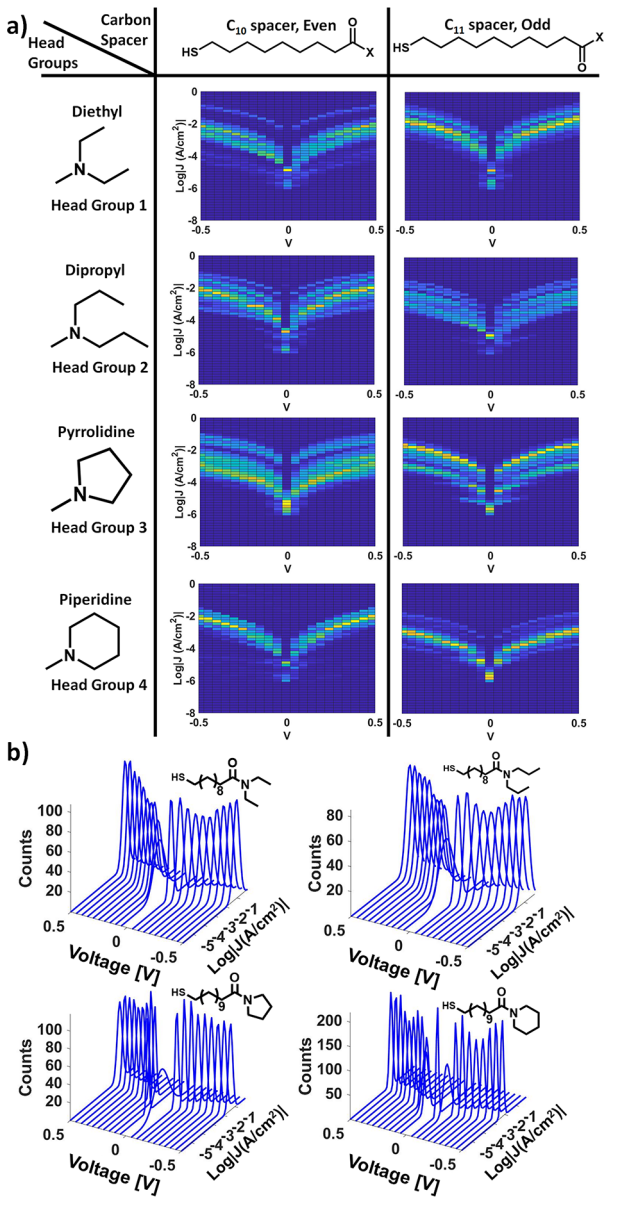

Figure 2. (a) Heat maps of all the data revealing similar current density but different distributions for different molecules. (b) Selected Gaussian plot fitted over all biases to show the distribution of current traces.

Effect of Spacer Parity: The Odd–Even Effect. Chain parity, the so-called odd–even effect, affects charge transport through SAMs.[2,7,13,17,18] To understand the effect of chain parity on the role of head group conformation in charge tunneling, we explore the response of the four head groups used in this study on an odd- or even-numbered spacer. First, we explore bias-dependent changes in distribution of the current density, i.e., characteristic of the Gaussian fits to current density at each voltage (Figure 3). For brevity and clarity, we use fits to the negative bias.

From a simple observation of the height (maxima) of these peaks, we note that the distribution in current density varies across the applied bias, illustrating an often-ignored parameter, bias-to-bias dependence. Comparing the C_2 analogues on a C_{10} spacer, we note that the open (diethyl, $\mathbf{1}^{E}$) moiety has a minimum at ∼0.3 V, while the closed (pyrrolidine, $\mathbf{3}^{E}$) analogue has a maximum at 0.15 V (Figure 3a). The C_3 ($\mathbf{2}^{E}$ and $\mathbf{4}^{E}$) analogues show a small dip at 0.2 V on an otherwise uniform distribution. When the spacer is changed to a C_{11} (Figure 3b), only $\mathbf{3}^{O}$ shows a similar trend to $\mathbf{3}^{E}$. The analogous $\mathbf{1}^{O}$ shows an asymptotic trend that plateaus at ca. 0.3 V. Analogous open-chain $\mathbf{2}^{O}$, however, shows the inverse behavior, in that at very low bias the distribution is sharper but rapidly drops to a plateau with an increase in voltage. Given the complexity in the trends, quantitative analysis of the trends in distributions was warranted. We inferred that changes in the coherence (peakedness) cannot be revealed through the low statistical moments (mean and variance) but can be revealed by trends in higher moments like skewness, *S*, and kurtosis, *K*.

Effect of Head Group on Bias-Dependent Behaviors. To quantify observed changes in current with changes in head group, we compared trends in skewness and kurtosis with changes in voltage. Figure 4 summarizes all the skewness and kurtosis data, and for brevity, a replot (without the data points) of these data is given alongside each plot for clarity. With increasing applied bias, an increasing trend in both skewness and kurtosis of current densities can be observed for most molecules. For molecule with a C_{10} (Even) spacer, head group 4 showed the largest increase over the ±0.5 V bias range, while head group 3 hardly showed any change in both skewness and kurtosis. Headgroup 1, however, showed a direction-dependent behavior at low bias range. With a C_{11} (odd) spacer, aside from head group 1, an increase in skewness and kurtosis over the bias range is lower than on the even series. Headgroup 4

https://doi.org/10.1021/jacs.1c06622
J. Am. Chem. Soc. 2021, 143, 13878–13886

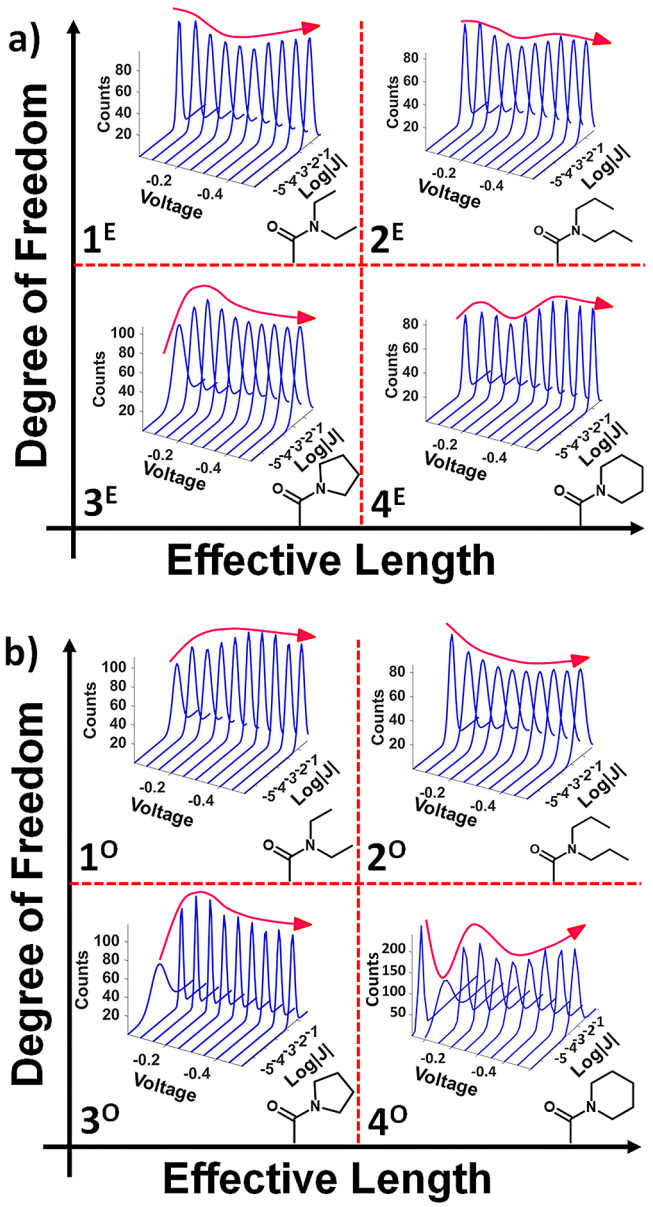

Figure 3. Effect of head group in current density distributions. (a) Gaussian plots for $HS(CH_2)_{10}CO$-R molecules and (b) Gaussian plots for $HS(CH_2)_{11}CO$-R analogues. A highlight of the general progression in the Gaussian mean is given as a guide to the eye.

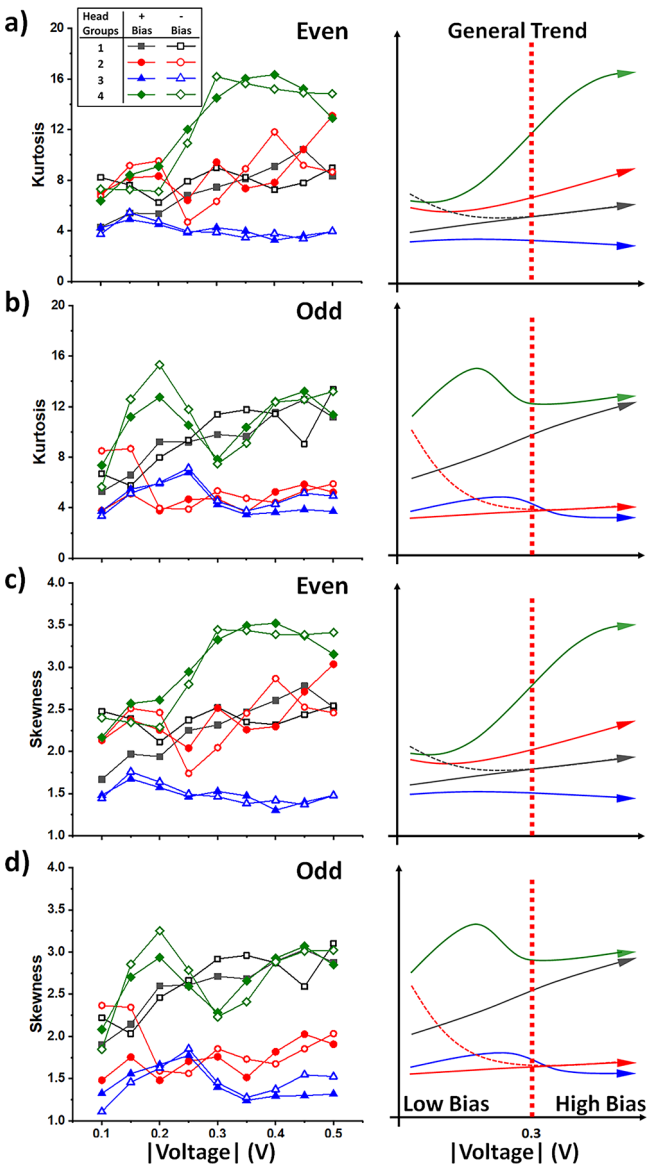

Figure 4. (a,b) Kurtosis of all molecules separated based on the direction of applied bias and their general trends without the data points. (c,d) Skewness of all molecules separated based on the direction of applied bias and their general trends highlighted.

showed a zigzag trend at low bias, but the increase in skewness and kurtosis is still low compared to other head groups.

Further analysis revealed more details on the bias-dependent changes occurring in conductivity during the measurement. As shown in Figure 4a−4d, molecules with head group 3 (pyrrolidine) showed less bias-dependent changes in both *S* and *K*. For head group 3, skewness remained at ∼1, while kurtosis was ∼4. This limited fluctuation could be related to this moiety having a limited number of conformations or ease of interconversion between the groups. This inference is further confirmed by the number of conformers and average energy to interconvert (0.67 Ha) observed from theoretical simulations of the head groups (Supporting Information Table S1). We observe that the analogous open-chain C_2 (head group 1) amide on a C_{11} spacer (Figure 4b,d) shows similar behavior after 0.2 V, with the lower voltage divergence being due to higher conductivity when the top electrode is positively biased. With a C_{10} (even) spacer, the diethyl amide shows a slight increase in *S* and *K* with bias with statistically insignificant fluctuations due to direction of current flow. The dipropyl (head group 2) amide also shows a gradual increase in *S* and *K* with an initial low-bias divergence for the C_{10} spacer.

The piperidine (head group 4), however, showed the most dynamic behavior in *S* and *K*. For molecule $\mathbf{4}^{E}$, an initial plateau (0−0.2 V) is observed followed by a gradual rise with a second plateau at ∼0.35 V. In the case of a C_{11} spacer, *S* and *K* show a peak (0.1−0.3 V) with a maximum at 0.2 V, followed by a gradual increase with increase in bias. The difference in trends in *S* and *K* for the C_2 vs C_3 analogues suggests that an increase in conformational degrees of freedom can influence the nature of current density distributions with each sweep (0 → ±0.5), capturing a series of independent responses likely dependent on the energy experienced by the molecule. On top of the bias-dependent trends, we observe that there exists a

https://doi.org/10.1021/jacs.1c06622
J. Am. Chem. Soc. 2021, 143, 13878−13886

convergence point around 0.3 V, where trends that dominated the low bias regions (split between + and − bias or zigzag) disappear, and both *S* and *K* start to converge irrespective of the direction of applied field.

The complexity in trends of *S* and *K*, coupled with the low range of energies needed to oscillate between conformers (<10 Ha), may lead to a significant number of chaos (randomness) and outliers. Lag plot of the obtained data (Figure 5) indicates

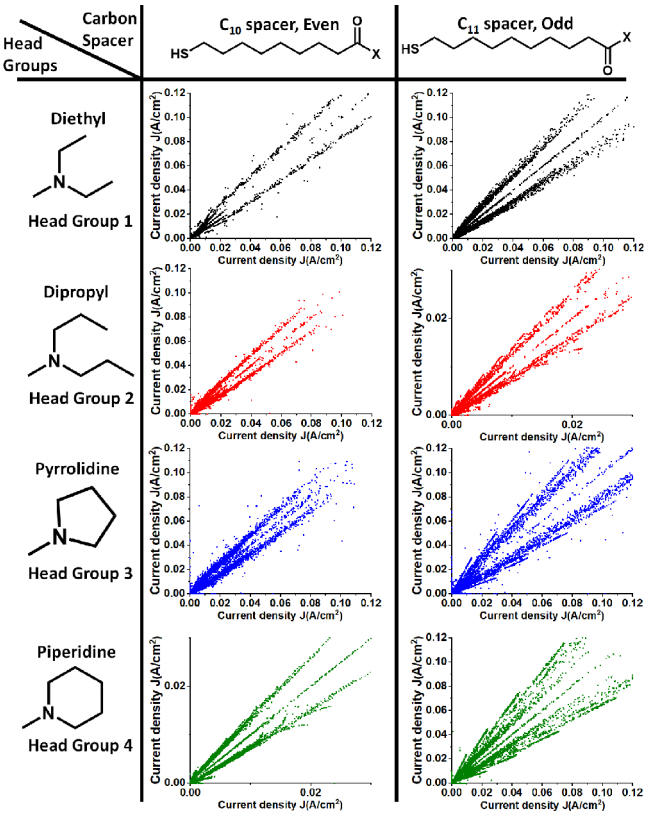

Figure 5. Lag plots for tunneling rates across SAMs. Two prominent serial correlations dominate data trends are observed irrespective of the nature of the head group. Weak correlations are observed with head group 4 on an odd spacer. The presence of a few off-diagonal data points indicates low number of outliers and the nonrandom nature of the data.

serial correlation (data not random) and a limited number of outliers. Molecules analyzed in this work, on the contrary to what we have observed in the past,[18] showed multiple traces instead of one linear narrow distribution. Two main symmetric traces surrounding one weak trace between them can be observed for all of the molecules analyzed (Figure 5). The C_{11} spacer (right column) generally showed more dispersed distribution than a C_{10} spacer, suggesting that the orientation of the head group is important in data distribution. This observation, and the divergent nature of the correlated data in the lag plots, combined with previous reports,[17,40] lead us to infer that the SAMs, under a changing applied field, should be considered a dynamic system contrary to the commonly adopted view that it is a static barrier. Given the complexity in trends observed above, we segregate the molecules based on the alkyl chain spacers and quantify the contribution of each structural variation on current density by applying the population-independent unpaired mean differences.

Quantifying Effect of Head Groups. Although the nature of the Gaussian distributions points to significant differences in charge-tunneling characteristics, we desired to quantify the effect of the spacer vis-à-vis the head group. Given the large number of molecules sampled (high population) per junction, we adopt the population-independent estimation plots (swarm plot, one-way ANOVA, and unpaired mean difference, $\Delta\mu$). Compared to *n*-alkanethiolate SAMs, all amides on an even alkyl spacer showed slightly enhanced (avg. $\Delta\mu$ = 0.41) conductivity (Figure 6a), while those on an odd spacer showed diminished (avg. $\Delta\mu$= −1.88) conductivity (Figure 6b). A zigzag fluctuation is observed from head group 1 to 4, as larger head groups lead to a more pronounced effect on conductivity. The diethyl (head group 1), depending on the alkyl spacer parity, can lead to either an increase in log (*J*) = 0.26 or a decrease (−1.49). The dipropyl (head group 2), similarly, lead to an increase in log (*J*) = 0.54 or a decrease (−2.11) depending on the spacer parity. Closed analogues showed similar trends, as pyrrolidine (head group 3) leads to a change in log (*J*) = +0.16 and −1.21, respectively, while piperidine (head group 4) gives a change in log (*J*) = +0.67 and −2.7 respectively (Figure 6c).

We have previously shown that dipole orientation affects charge tunneling across SAM-based molecular junctions.[18] We hypothesized that the difference caused by the alkyl chain spacers may be due to conformation-driven changes to the orientation of the overall molecular dipole. We, however, exercise caution to avoid over-interpretation of the results as parity also affects head group orientation that can also affect the coupling with the top electrode. To normalize the effect of dipole orientation and separate the effect of head group, we calculate the difference of $\Delta\mu$ between the 2 types of alkyl chain spacers. We note that pyrrolidine showed the smallest change in $\Delta\mu$ across the spacers (1.37), followed by diethyl (1.75), dipropyl (2.65), and piperidine (3.37) (Figure 6d). This large difference for homologous molecules points to the impact of the head group on tunneling characteristics of the junction, and more attention should be paid to conformational freedom in these junctions. We infer that the correlation between magnitudes captured in Figure 6d to conformational versatility (Supporing information Table S1) suggest a need to further investigate conformational effects.

CONCLUSION

From comparison of charge-tunneling behaviors between amide molecules with the same chain length and different conformation degree of freedom, we may infer the following.

a. Charge Transport Across Amide-Based SAMs Is a Multidimensional Problem. Each component of the system, including the carbon backbone, amide group, head group, and top electrode interface, affects the charge-tunneling behavior of SAMs. As illustrated above, similar moieties can either enhance or hinder tunneling. The underlying mechanism is not yet understood and is beyond the scope of the current work. The bias-dependent fluctuation in current density illustrates the dynamic nature of the system, raising the need for more detailed and whole bias-range analysis as opposed to using a single bias as a representative of the whole. The use of population-independent statistics (estimation plots) further enables clear delineation of subtle but important contribution as illustrated here.

b. Charge Transport Behavior of Amide-Based SAMs Is Affected by the Head Group of the Molecule. The

https://doi.org/10.1021/jacs.1c06622
J. Am. Chem. Soc. 2021, 143, 13878−13886

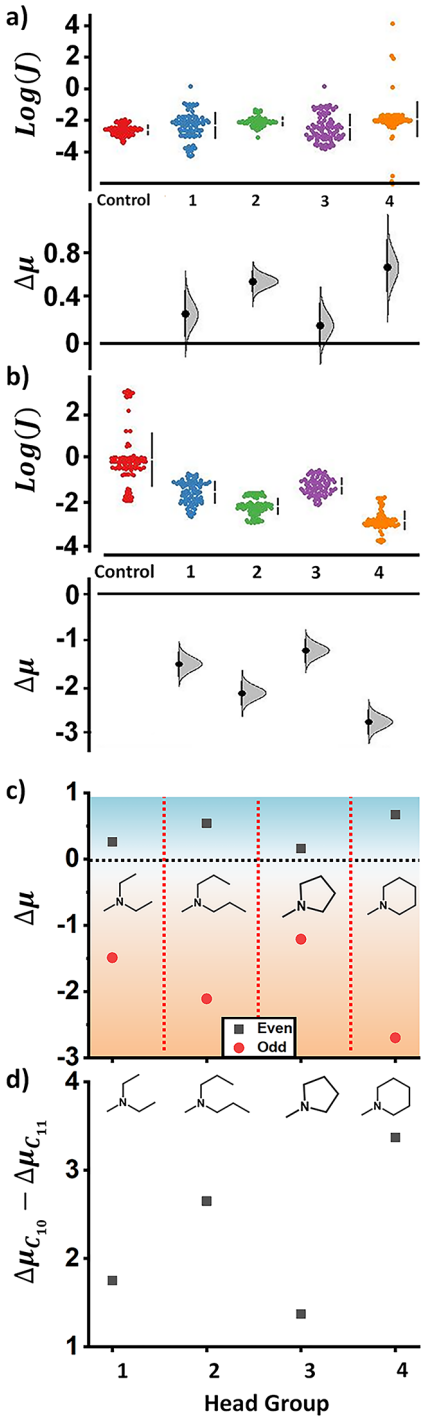

Figure 6. Effect of head group on charge-tunneling rate across SAMs at 95% confidence interval. (a) On C_{10}-based molecules, the head group leads to an increase in charge-tunneling rate. (b) On C_{11}-based molecules, the head groups lead to a decrease in charge-tunneling rate. (c) Comparative summary of effect of head group on conductivity on both C_{10}-based and C_{11}-based molecules as captured by the unpaired mead difference. (d) Capturing the effect of the head group on the spacer parity using differences in unpaired mean differences of the same head group but on different spacers.

conductivity, as well as bias-dependent stability of junctions, are significantly perturbed by the head group. This perturbation amplifies the odd−even effect where an increase or decrease in tunneling was observed for all amides investigated here. We observe that this perturbation aligns with head group degree of freedom and associated volumetric change and follows the order **4** > **2** > **1** > **3** for head groups investigated here. These results further inform the role of supramolecular structure in charge tunneling.[14,15,41]

c. Conformation Changes Can Affect Charge Transport Behavior of SAMs. Related to (b) above, we observed that both skewness and kurtosis show bias-dependent behaviors which could be attributed to both the dipole-field interaction and/or joule heating related conformational changes. By comparing data collected from molecules with the same head group but a different alkyl spacer, we infer that the supramolecular nature of the SAM significantly perturbs the current density as previously noted in molecular rectifiers.[14,19,42]

d. Charge Tunneling Rate at Fixed Bias Is Not Accurately Representative of SAMs as a dynamic Charge Tunneling System. Given the dynamic, nonlinear nature of SAM-based molecular junctions, it is impossible to capture all the dynamic changes caused by a changing applied field with one fixed bias. It is therefore necessary to report current density and distribution characteristics at each bias. Heat maps and 3D Gaussian distributions have emerged as good all-data presentation methods, but these should be supplemented with trends in distribution skew and kurtosis.

e. Population-Independent Estimation Plots Are a Powerful Tool in Delineating Complex Molecular Properties. Due to the number of repeated traces, traditional *p*-value-based statistical analysis would often lead to an unrealistically small confidence band, which would result in false rejection of the null hypothesis. In order to correct this issue, we used estimation plots to capture the difference and quantify the contribution of different parameters in charge transport.[43] Earlier studies on amides using *p*-values and lower statistical moments concluded that amides do not significantly affect tunneling currents and are therefore comparable to hydrocarbon analogs. Herein, and in earlier communications, we show that, looking at complete data sets coupled with higher statistical moments and estimation plots, contributions of subtle molecular changes can be revealed.

■ ASSOCIATED CONTENT

Supporting Information

The Supporting Information is available free of charge at https://pubs.acs.org/doi/10.1021/jacs.1c06622.

Experimental procedures for molecule synthesis and characterization data for all molecules (PDF)

Movie illustrating the structure of Head-1 (MP4)

Movie illustrating the structure of Head-2 (MP4)

Movie illustrating the structure of Head-3 (MP4)

Movie illustrating the structure of Head-4 (MP4)

■ AUTHOR INFORMATION

Corresponding Author

Martin Thuo − *Department of Materials Science and Engineering, Iowa State University, Ames, Iowa 50011, United States; Micro-Electronic Research Center, Iowa State University, Ames, Iowa 50011, United States; Biopolymer and Biocomposites Research Team, Center for Bioplastics and Biocomposites, Iowa State University, Ames, Iowa 50011, United States;* orcid.org/0000-0003-3448-8027; Email: mthuo@iastate.edu

Authors

Chuanshen Du − *Department of Materials Science and Engineering, Iowa State University, Ames, Iowa 50011, United States*

Sean R. Norris − *Department of Chemistry, Iowa State University, Ames, Iowa 50011-3111, United States;* orcid.org/0000-0003-3248-2094

Abhishek Thakur − *Department of Chemistry, University of Miami, Coral Gables, Florida 33146, United States*

Jiahao Chen − *Department of Materials Science and Engineering, Iowa State University, Ames, Iowa 50011, United States; Micro-Electronic Research Center, Iowa State University, Ames, Iowa 50011, United States;* orcid.org/0000-0001-7563-8023

Brett VanVeller − *Department of Chemistry, Iowa State University, Ames, Iowa 50011-3111, United States;* orcid.org/0000-0002-3792-0308

Complete contact information is available at: https://pubs.acs.org/10.1021/jacs.1c06622

Author Contributions

The manuscript was written through contributions of all authors. All authors have given approval to the final version of the manuscript.

Notes

The authors declare no competing financial interest.

■ ACKNOWLEDGMENTS

This work was supported in part by the U.S. Air Force Office of Scientific Research under award number FA2386-16-1-4113 and a Catron fellowship to J.C. S.N. and B.V.V. were supported by National Science Foundation, Division of Chemistry, award number 1848261.

■ REFERENCES

(1) Belding, L.; Root, S. E.; Li, Y.; Park, J.; Baghbanzadeh, M.; Rojas, E.; Pieters, P. F.; Yoon, H. J.; Whitesides, G. M. Conformation, and Charge Tunneling through Molecules in SAMs. *J. Am. Chem. Soc.* **2021**, *143* (9), 3481−3493.

(2) Chen, J.; Giroux, T. J.; Nguyen, Y.; Kadoma, A. A.; Chang, B. S.; VanVeller, B.; Thuo, M. M. Understanding interface (odd−even) effects in charge tunneling using a polished EGaIn electrode. *Phys. Chem. Chem. Phys.* **2018**, *20* (7), 4864−4878.

(3) Nurbawono, A.; Liu, S.; Nijhuis, C. A.; Zhang, C. Odd−Even Effects in Charge Transport through Self-Assembled Monolayer of Alkanethiolates. *J. Phys. Chem. C* **2015**, *119* (10), 5657−5662.

(4) Wang, Z.; Chen, J.; Oyola-Reynoso, S.; Thuo, M. The Porter-Whitesides discrepancy: Revisiting odd-even effects in wetting properties of n-alkanethiolate SAMs. *Coatings* **2015**, *5* (4), 1034−1055.

(5) Wang, Z.; Chen, J.; Gathiaka, S. M.; Oyola-Reynoso, S.; Thuo, M. Effect of Substrate Morphology on the Odd−Even Effect in Hydrophobicity of Self-Assembled Monolayers. *Langmuir* **2016**, *32* (40), 10358−10367.

(6) Newcomb, L. B.; Tevis, I. D.; Atkinson, M. B.; Gathiaka, S. M.; Luna, R. E.; Thuo, M. Odd−even effect in the hydrophobicity of n-alkanethiolate self-assembled monolayers depends upon the roughness of the substrate and the orientation of the terminal moiety. *Langmuir* **2014**, *30* (40), 11985−11992.

(7) Baghbanzadeh, M.; Simeone, F. C.; Bowers, C. M.; Liao, K.-C.; Thuo, M.; Baghbanzadeh, M.; Miller, M. S.; Carmichael, T. B.; Whitesides, G. M. Odd−even effects in charge transport across n-alkanethiolate-based SAMs. *J. Am. Chem. Soc.* **2014**, *136* (48), 16919−16925.

(8) Akkerman, H. B.; Mannsfeld, S. C.; Kaushik, A. P.; Verploegen, E.; Burnier, L.; Zoombelt, A. P.; Saathoff, J. D.; Hong, S.; Atahan-Evrenk, S.; Liu, X.; et al. Effects of odd−even side chain length of alkyl-substituted diphenylbithiophenes on first monolayer thin film packing structure. *J. Am. Chem. Soc.* **2013**, *135* (30), 11006−11014.

(9) Reus, W. F.; Thuo, M. M.; Shapiro, N. D.; Nijhuis, C. A.; Whitesides, G. M. The SAM, not the electrodes, dominates charge transport in metal-monolayer//Ga_2O_3/Gallium−Indium eutectic junctions. *ACS Nano* **2012**, *6* (6), 4806−4822.

(10) Ramin, L.; Jabbarzadeh, A. Odd−even effects on the structure, stability, and phase transition of alkanethiol self-assembled monolayers. *Langmuir* **2011**, *27* (16), 9748−9759.

(11) Liu, Z.; Kobayashi, M.; Paul, B. C.; Bao, Z.; Nishi, Y. Contact engineering for organic semiconductor devices via Fermi level depinning at the metal-organic interface. *Phys. Rev. B: Condens. Matter Mater. Phys.* **2010**, *82* (3), 035311.

(12) Wang, Z.; Chen, J.; Oyola-Reynoso, S.; Thuo, M. Empirical evidence for roughness-dependent limit in observation of odd−even effect in wetting properties of polar liquids on n-alkanethiolate self-assembled monolayers. *Langmuir* **2016**, *32* (32), 8230−8237.

(13) Thuo, M. M.; Reus, W. F.; Nijhuis, C. A.; Barber, J. R.; Kim, C.; Schulz, M. D.; Whitesides, G. M. Odd−even effects in charge transport across self-assembled monolayers. *J. Am. Chem. Soc.* **2011**, *133* (9), 2962−2975.

(14) Song, P.; Yuan, L.; Roemer, M.; Jiang, L.; Nijhuis, C. A. Supramolecular vs electronic structure: The effect of the tilt angle of the active group in the performance of a molecular diode. *J. Am. Chem. Soc.* **2016**, *138* (18), 5769−5772.

(15) Thompson, D.; Nijhuis, C. A. Even the odd numbers help: failure modes of SAM-based tunnel junctions probed via odd-even effects revealed in synchrotrons and supercomputers. *Acc. Chem. Res.* **2016**, *49* (10), 2061−2069.

(16) Thuo, M. M.; Reus, W. F.; Simeone, F. C.; Kim, C.; Schulz, M. D.; Yoon, H. J.; Whitesides, G. M. Replacing -CH_2CH_2- with -CONH- Does Not Significantly Change Rates of Charge Transport through Ag^{TS}-SAM//Ga_2O_3/EGaIn Junctions. *J. Am. Chem. Soc.* **2012**, *134* (26), 10876−10884.

(17) Chen, J.; Kim, M.; Gathiaka, S.; Cho, S. J.; Kundu, S.; Yoon, H. J.; Thuo, M. M. Understanding Keesom Interactions in Monolayer-Based Large-Area Tunneling Junctions. *J. Phys. Chem. Lett.* **2018**, *9* (17), 5078−5085.

(18) Chen, J.; Gathiaka, S.; Wang, Z.; Thuo, M. Role of Molecular Dipoles in Charge Transport across Large Area Molecular Junctions Delineated Using Isomorphic Self-Assembled Monolayers. *J. Phys. Chem. C* **2017**, *121* (43), 23931−23938.

(19) Nerngchamnong, N.; Yuan, L.; Qi, D.-C.; Li, J.; Thompson, D.; Nijhuis, C. A. The role of van der Waals forces in the performance of molecular diodes. *Nat. Nanotechnol.* **2013**, *8* (2), 113−118.

(20) Carlotti, M.; Kovalchuk, A.; Wächter, T.; Qiu, X.; Zharnikov, M.; Chiechi, R. C. Conformation-driven quantum interference effects mediated by through-space conjugation in self-assembled monolayers. *Nat. Commun.* **2016**, *7* (1), 1−7.

(21) Chen, X.; Hu, H.; Trasobares, J.; Nijhuis, C. A. Rectification ratio and tunneling decay coefficient depend on the contact geometry revealed by in situ imaging of the formation of EGaIn junctions. *ACS Appl. Mater. Interfaces* **2019**, *11* (23), 21018−21029.

(22) Vilan, A. Analyzing molecular current-voltage characteristics with the Simmons tunneling model: scaling and linearization. *J. Phys. Chem. C* **2007**, *111* (11), 4431−4444.

(23) Akkerman, H. B.; Naber, R. C.; Jongbloed, B.; van Hal, P. A.; Blom, P. W.; de Leeuw, D. M.; de Boer, B. Electron tunneling through alkanedithiol self-assembled monolayers in large-area molecular junctions. *Proc. Natl. Acad. Sci. U. S. A.* **2007**, *104* (27), 11161−11166.

(24) Hill, C. M.; Kim, J.; Bard, A. J. Electrochemistry at a metal nanoparticle on a tunneling film: a steady-state model of current densities at a tunneling ultramicroelectrode. *J. Am. Chem. Soc.* **2015**, *137* (35), 11321−11326.

(25) Brinkman, W.; Dynes, R.; Rowell, J. Tunneling conductance of asymmetrical barriers. *J. Appl. Phys.* **1970**, *41* (5), 1915−1921.
(26) Wang, W.; Lee, T.; Reed, M. A. Mechanism of electron conduction in self-assembled alkanethiol monolayer devices. *Phys. Rev. B: Condens. Matter Mater. Phys.* **2003**, *68* (3), 035416.
(27) Pakiari, A.; Jamshidi, Z. Nature and strength of M− S Bonds (M= Au, Ag, and Cu) in binary alloy gold clusters. *J. Phys. Chem. A* **2010**, *114* (34), 9212−9221.
(28) Jia, C.; Guo, X. Molecule−electrode interfaces in molecular electronic devices. *Chem. Soc. Rev.* **2013**, *42* (13), 5642−5660.
(29) Xie, Z.; Bâldea, I.; Smith, C. E.; Wu, Y.; Frisbie, C. D. Experimental and theoretical analysis of nanotransport in oligophenylene dithiol junctions as a function of molecular length and contact work function. *ACS Nano* **2015**, *9* (8), 8022−8036.
(30) Jiang, L.; Sangeeth, C. S.; Wan, A.; Vilan, A.; Nijhuis, C. A. Defect scaling with contact area in EGaIn-based junctions: impact on quality, Joule heating, and apparent injection current. *J. Phys. Chem. C* **2015**, *119* (2), 960−969.
(31) Sporrer, J.; Chen, J.; Wang, Z.; Thuo, M. M. Revealing the Nature of Molecule−Electrode Contact in Tunneling Junctions Using Raw Data Heat Maps. *J. Phys. Chem. Lett.* **2015**, *6* (24), 4952−4958.
(32) Weiner, P. K.; Kollman, P. A. AMBER: Assisted model building with energy refinement. A general program for modeling molecules and their interactions. *J. Comput. Chem.* **1981**, *2* (3), 287−303.
(33) Wang, J.; Wolf, R. M.; Caldwell, J. W.; Kollman, P. A.; Case, D. A. Development and testing of a general Amber force field. *J. Comput. Chem.* **2004**, *25* (9), 1157−1174.
(34) Shao, J.; Tanner, S. W.; Thompson, N.; Cheatham, T. E. Clustering molecular dynamics trajectories: 1. Characterizing the performance of different clustering algorithms. *J. Chem. Theory Comput.* **2007**, *3* (6), 2312−2334.
(35) Thakur, A.; Somai, S.; Yue, K.; Ippolito, N.; Pagan, D.; Xiong, J.; Ellis, H. R.; Acevedo, O. Substrate-Dependent Mobile Loop Conformational Changes in Alkanesulfonate Monooxygenase from Accelerated Molecular Dynamics. *Biochemistry* **2020**, *59* (38), 3582−3593.
(36) Chen, J.; Wang, Z.; Oyola-Reynoso, S.; Thuo, M. M. Properties of Self-Assembled Monolayers Revealed via Inverse Tensiometry. *Langmuir* **2017**, *33* (47), 13451−13467.
(37) Chen, J.; Chang, B.; Oyola-Reynoso, S.; Wang, Z.; Thuo, M. Quantifying Gauche defects and phase evolution in self-assembled monolayers through sessile drops. *ACS omega* **2017**, *2* (5), 2072−2084.
(38) Love, J. C.; Estroff, L. A.; Kriebel, J. K.; Nuzzo, R. G.; Whitesides, G. M. Self-assembled monolayers of thiolates on metals as a form of nanotechnology. *Chem. Rev.* **2005**, *105* (4), 1103−1170.
(39) Ulman, A. Formation and structure of self-assembled monolayers. *Chem. Rev.* **1996**, *96* (4), 1533−1554.
(40) Nerngchamnong, N.; Wu, H.; Sotthewes, K.; Yuan, L.; Cao, L.; Roemer, M.; Lu, J.; Loh, K. P.; Troadec, C.; Zandvliet, H. J. W.; Nijhuis, C. A. Supramolecular Structure of Self-Assembled Monolayers of Ferrocenyl Terminated n-Alkanethiolates on Gold Surfaces. *Langmuir* **2014**, *30* (44), 13447−13455.
(41) Jiang, L.; Sangeeth, C. S.; Yuan, L.; Thompson, D.; Nijhuis, C. A. One-nanometer thin monolayers remove the deleterious effect of substrate defects in molecular tunnel junctions. *Nano Lett.* **2015**, *15* (10), 6643−6649.
(42) Chen, X.; Roemer, M.; Yuan, L.; Du, W.; Thompson, D.; Del Barco, E.; Nijhuis, C. A. Molecular diodes with rectification ratios exceeding 10^5 driven by electrostatic interactions. *Nat. Nanotechnol.* **2017**, *12* (8), 797−803.
(43) Ho, J.; Tumkaya, T.; Aryal, S.; Choi, H.; Claridge-Chang, A. Moving beyond P values: data analysis with estimation graphics. *Nat. Methods* **2019**, *16* (7), 565−566.

https://doi.org/10.1021/jacs.1c06622
J. Am. Chem. Soc. 2021, 143, 13878−13886